RSC Advances

PAPER

View Article Online
View Journal | View Issue

Cite this: *RSC Adv.*, 2026, **16**, 1988

Merging dynamic and static chirality in propeller-shaped carbazole oligomers *via* chiral amine substitution

Yuma Tanioka,[a] Ryosuke Omasa,[a] Tetsuo Okujima,[ab] Hidemitsu Uno[a] and Masayoshi Takase *[ab]

Received 26th November 2025
Accepted 23rd December 2025

DOI: 10.1039/d5ra09136e

rsc.li/rsc-advances

Organic emissive materials exhibiting circularly polarized luminescence (CPL) have attracted considerable attention as promising candidates for next-generation photonic and electronic devices. However, most CPL-active molecules require laborious procedures such as asymmetric synthesis or optical resolution. In this study, chiral propeller-shaped molecules were conveniently synthesized by introducing chiral amines possessing static chirality into a dynamically chiral propeller framework. The molecule was obtained *via* a two-step aromatic nucleophilic substitution (S_NAr) sequence and exhibited distinct CPL activity ($|g_{lum}| \approx 2.0 \times 10^{-3}$ at room temperature) without optical resolution. Furthermore, a bifunctionalized derivative employing a chiral diamine with a similar substructure was synthesized, but no enhancement in CPL anisotropy was observed. These results indicate that precise control over the relative orientation of the magnetic and electric transition dipole moments is crucial for improving CPL performance.

Introduction

Circularly polarized luminescence (CPL)-active organic materials have attracted considerable attention owing to their promising applications in emerging technologies such as 3D displays,[1] quantum communication,[2,3] and bioimaging.[4] A wide variety of CPL-active molecules have been developed to date, typically represented by helicenes,[5,6] twistacenes,[7] and distorted polycyclic aromatic hydrocarbons.[8] Their chirality originates from twisted molecular frameworks arising from steric strain. When the inversion barrier is sufficiently low, interconversion between the two enantiomeric conformations becomes feasible, leading to so-called "dynamic chirality".[9] Although dynamic chirality has been exploited in the development of molecular chirality switches, achieving both reversible interconversion and structural stability remains a persistent challenge.[10–12]

To address this issue, various molecular design strategies have been investigated. These include extending helical π-conjugated systems to increase the inversion barrier,[13–15] and introducing bulky substituents into polycyclic aromatic frameworks to sterically lock the chiral conformation.[16–18] However, such approaches typically require laborious procedures involving asymmetric synthesis or the separation of racemates.[14,19] Recent studies have demonstrated that these challenges can be more efficiently overcome by coupling dynamic chiral units with conformationally rigid, static chiral moieties.[10,20–26] Despite its conceptual simplicity, this approach has remained surprisingly underexplored.

Propeller-shaped molecules such as hexaarylbenzenes (HABs) represent an attractive platform for such molecular design. Owing to the steric congestion among the six peripheral aryl blades, HABs adopt a propeller-like geometry. In the idealized HAB structure, each blade is twisted by approximately 60° relative to the central benzene core, generating two atropisomers (Fig. 1). In parent HABs, both conformers are energetically equivalent, rendering the molecule achiral. In contrast,

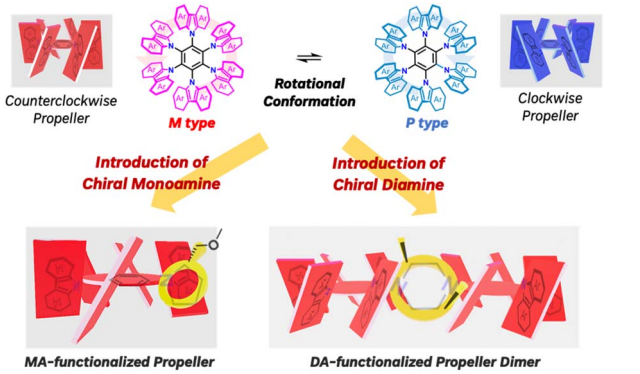

Fig. 1 Schematic illustrations of propeller chirality, and MA (monoamine)-functionalized propeller and DA (diamine)-functionalized propeller dimer studied in this work.

[a]*Graduate School of Science and Engineering, Ehime University, Matsuyama 790-8577, Japan. E-mail: takase.masayoshi.ry@ehime-u.ac.jp*
[b]*Research Unit on Molecular Materials Science for Toroidal π-Electron Systems, Ehime University, Matsuyama 790-8577, Japan*

the introduction of chiral auxiliaries can bias the torsional sense of the blades through steric interactions, thereby giving rise to distinct propeller chirality.[27–30] Thus, the HAB skeleton serves as a versatile scaffold that exhibits controllable dynamic chirality.

In this context, we previously developed a propeller-shaped molecule, Bz-6PDI, composed of a benzene core bearing six perylene diimide blades, in which all blades are equipped with conformationally stable chiral units.[30] Bz-6PDI was conveniently synthesized *via* an aromatic nucleophilic substitution (S_NAr) reaction with hexafluorobenzene and exhibited solvent-induced chirality inversion along with CPL activity at room temperature. Despite its relative simplicity, this approach still required the pre-synthesis of chiral blades bearing stable chiral units, and therefore remained somewhat limited in practicality.

In this work, we aimed to achieve facile fixation of molecular chirality by merging dynamic and static chiral elements within an HAB framework (Fig. 1). To this end, chiral amines were introduced into the blade positions of the HAB core, employing carbazole—a well-known and versatile building block—as the aryl component.[31–33] Readily available chiral amines served as the source of static chirality. The target monoamine (MA)-functionalized molecule **1** was synthesized through a two-step S_NAr sequence using enantiopure amine. As expected, (*R*/*S*)-**1** exhibited both circular dichroism (CD) and CPL activity ($|g_{lum}| = 2.0 \times 10^{-3}$ at room temperature) without optical resolution. Furthermore, the dimeric derivative (*R*,*R*/*S*,*S*)-**2**, in which two carbazole oligomers were connected *via* a diamine linker, also displayed CD and CPL responses with a slightly reduced anisotropy factor ($|g_{lum}| = 1.0 \times 10^{-3}$ at room temperature). Taken together, these findings demonstrate that the covalent coupling of dynamic and static chiral units represents an effective and synthetically simple strategy for achieving stable molecular chirality and pronounced CPL activity.

Results and discussion

Synthesis

To construct propeller-shaped chiral molecules, we selected 2-(methoxymethyl)pyrrolidine (**3**) as a chiral auxiliary owing to its commercial availability and high nucleophilicity. Both enantiomers, (*R*)-**1** and (*S*)-**1**, were obtained in moderate yields through a two-step S_NAr sequence (Scheme 1).[34] The first step involved the S_NAr reaction of chiral amine **3** with hexafluorobenzene to afford the mono-substituted intermediate **4**. Subsequent S_NAr substitution under basic conditions using calcium hydride as the base[35,36] furnished the desired product **1**. In the ^1H NMR spectrum of **1** in $C_2D_2Cl_4$, the aromatic proton signals appeared broadened at room temperature, reflecting both low molecular symmetry and internal motion within the propeller framework. Upon heating, these signals sharpened and became more resolved in $C_2D_2Cl_4$, indicating a thermally activated conformational process (Fig. S3a).

For the synthesis of the dimeric derivative, *cis*-2,5-dimethylpiperazine (**6**) was chosen as a linker because it is readily accessible and provides a chiral framework analogous to that of monomeric **3**. According to a reported procedure,[37] the

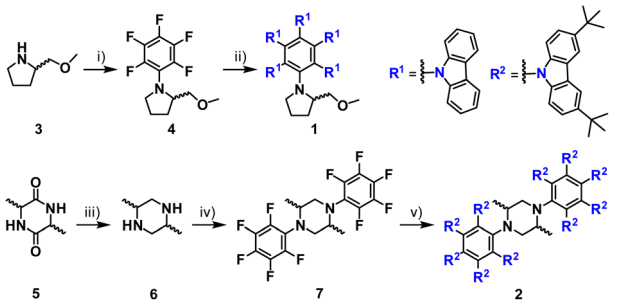

Scheme 1 Synthetic scheme of (*R*/*S*)-**1** and (*R*,*R*/*S*,*S*)-**2**. Reagents and conditions: (i) *n*-BuLi, C_6F_6, THF, −78 °C, (*R*)-**4**: 72%, (*S*)-**4**: 56%; (ii) carbazole, CaH_2, DMAc, 160 °C, (*R*)-**1**: 50%, (*S*)-**1**: 63%; (iii) $LiAlH_4$, THF, reflux, (*R*,*R*)-**6**: 91%, (*S*,*S*)-**6**: 89%; (iv) *n*-BuLi, C_6F_6, THF, −78 °C, (*R*,*R*)-**7**: 75%, (*S*,*S*)-**7**: 79%; (v) 3,6-di-*t*-Bu-carbazole, CaH_2, DMAc, 160 °C, (*R*,*R*)-**2**: 70%, (*S*,*S*)-**2**: 68%.

piperazine precursor, diketopiperazine **5**, was prepared, and subsequently reduced with $LiAlH_4$ to yield the chiral diamine **6**. Attempts to synthesize the dimer **2** using parent carbazole, following a similar S_NAr strategy to that used for **1**, were unsuccessful due to the extremely poor solubility of the resulting product, which hindered both the reaction progress and purification. To overcome this limitation, solubilizing substituents were introduced at the 3,6-positions of the carbazole units. The resulting dimer **2**, in which two carbazole pentamers were linked *via* the chiral piperazine-based linker, was successfully obtained through the same two-step S_NAr sequence employed for **1**. In the aromatic region of the ^1H NMR spectra of **2** in $CDCl_3$ and $C_2D_2Cl_4$, pronounced signal broadening was observed, and even upon heating, no significant improvement in resolution occurred in $C_2D_2Cl_4$ (Fig. S3b). In contrast, the signals corresponding to the piperazine framework remained sharp, suggesting the formation of a single, well-defined product. Furthermore, the absence of any detectable fluorine signals in the ^{19}F NMR spectrum confirmed complete substitution of all fluorine atoms by carbazole units, verifying the formation of the fully substituted derivative **2**.

Optical and chiroptical properties

The optical properties of **1** and **2** were evaluated in various solvents, including cyclohexane, dichloromethane (DCM), MeOH, and DMF (Fig. S4a, b and 2a). The UV-vis absorption spectra showed little dependence on solvent polarity, exhibiting a main absorption band around 340 nm with a shoulder peak near 360 nm. In contrast, the emission spectra displayed distinct solvent-dependent behavior, characteristic of carbazole-based architectures,[38,39] suggesting the involvement of an intramolecular charge-transfer (ICT) process. The absorption spectrum of **2** exhibited no appreciable red shift compared to that of **1** (Fig. 2a), indicating that π-conjugation was not significantly extended upon dimerization. However, the emission maxima of **2** were consistently red-shifted in all solvents examined (Fig. S4b), which can be attributed to increased structural flexibility arising from the linkage of two carbazole units *via* a diamine linker.

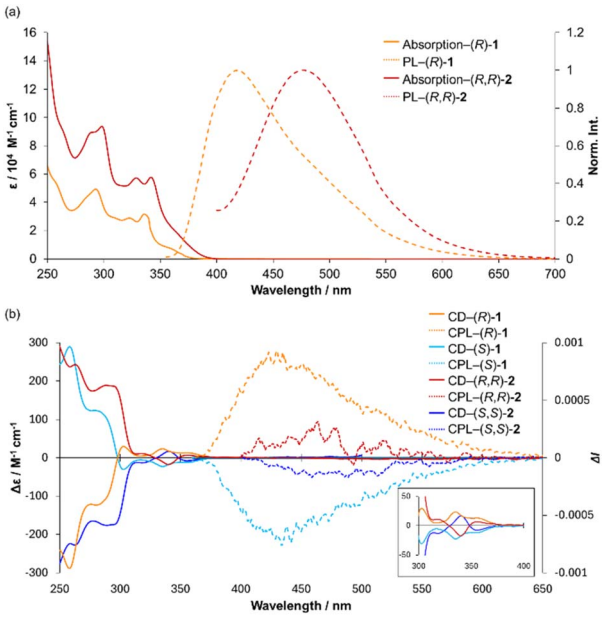

Fig. 2 (Chir)optical properties of (*R*/*S*)-**1** and (*R*,*R*/*S*,*S*)-**2**. (a) Absorption and PL spectra in DCM (λ_{ex} = 330 nm) and (b) CD and CPL spectra in DCM (λ_{ex} = 330 nm). The inset shows an enlarged view of the CD spectra over 300–400 nm.

Next, the influence of the chiral auxiliary on the chiroptical properties of these propeller-type molecules was examined by CD and CPL spectroscopy in DCM. Both **1** and **2** bearing the (*R*)-amine moiety displayed positive Cotton effects, whereas the corresponding (*S*)-enantiomers exhibited mirror-image negative cotton effects (Fig. 2b). In CPL measurements, **1** showed clear CPL activity with a $|g_{lum}|$ value of 2.0×10^{-3}. Dimer **2** also exhibited CPL signals, albeit with a smaller anisotropy factor of $|g_{lum}| = 1.0 \times 10^{-3}$. Interestingly, the $|g_{lum}|$ value of (*R*,*R*)-**2** was not simply additive relative to that of (*R*)-**1**; instead, its CPL intensity was reduced. This behavior can be rationalized from a structural perspective. In (*R*,*R*)-**2**, the two methyl groups on the central piperazine core adopt axial and equatorial orientations, respectively, leading to the loss of bilateral symmetry between the two propeller units. This asymmetry likely prevents the propeller helicities from aligning in the same sense, as observed for (*R*)-**1**, thereby diminishing the overall anisotropy of the system.

Solvent and temperature dependence of chiroptical response

The solvent- and temperature-dependent CD behaviors of (*R*)-**1** and (*R*,*R*)-**2** were subsequently investigated (Fig. 3 and S6c, d). Such analyses are highly informative for elucidating the dynamic nature of chiral propeller molecules.[30,40] As observed for previously reported propeller-type systems,[27,28,30] the CD intensity of (*R*)-**1** gradually decreased across the entire wavelength region upon heating. In contrast, no appreciable wavelength shift was detected within the examined temperature range. The absence of spectral shifts suggests that conformational changes involving torsional motion within the propeller framework are restricted, even under thermal perturbation.

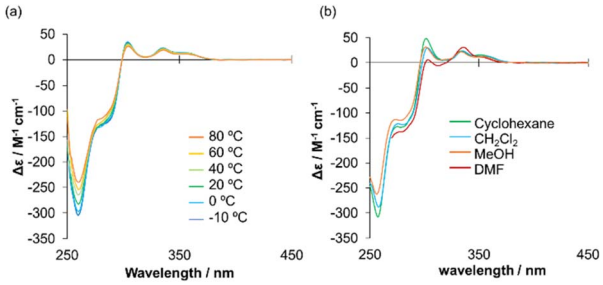

Fig. 3 CD spectra of (*R*)-**1** (a) at various temperatures in tetrachloroethane and (b) in various solvents at rt.

With respect to solvent effects, (*R*)-**1** exhibited comparable CD intensities in cyclohexane, DCM, MeOH, and DMF. This observation indicates that the chiroptical response is not governed solely by solvent polarity. Instead, it is likely influenced by a combination of factors such as solvent size, shape, and viscosity, all of which can modulate the conformational freedom and dynamic equilibrium of the propeller scaffold.

DFT calculations

To gain deeper insight into the above hypothesis, DFT calculations were carried out (Fig. 4). The molecular geometries of (*R*)-**1** and (*R*,*R*)-**2** were optimized at the B3LYP/6-31G(d) and B3LYP/6-31G levels, respectively. The CD spectra were then evaluated by TD-DFT at the B3LYP/6-31+G(d) level. The dissymmetry factor (*g* value) is defined as the vector product of the electric and magnetic transition dipole moments. For (*R*)-**1**, the angle between these two moments was calculated to be 1.9°, giving a cos θ value close to 1, which indicates that the two vectors are nearly parallel. In contrast, (*R*,*R*)-**2** exhibited an angle of 88.6°, implying that the two moments are almost orthogonal, thereby accounting for its smaller *g* value.

The calculated CD spectra further clarify the relationship between molecular geometry and chiroptical properties. In (*R*)-**1**, the rotational strength associated with the HOMO → LUMO transition is large (R_{vel} = 8.02), whereas in (*R*,*R*)-**2**, the longest-wavelength band, corresponding to the HOMO−1 → LUMO

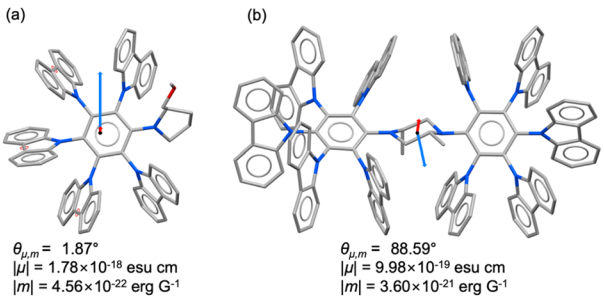

Fig. 4 Calculated transition dipole moments for the S0 → S1 electronic transitions in (a) (*R*)-**1** and (b) (*R*,*R*)-**2**. The electric transition dipole moments (μ) are shown in red, and the magnetic transition dipole moments (*m*) are shown in blue. Arrows for moments are displayed with 1 a.u. = 5.29 Å.

transition, shows a much smaller rotational strength (R_{vel} = 0.83). Moreover, both (*R*)-**1** and (*R*,*R*)-**2** display a characteristic pattern in which a large negative rotational strength at shorter wavelengths is followed by a positive one at longer wavelength (Fig. S5b). Accordingly, the absence of a negative CD signal in the 300–400 nm region for (*R*)-**1** can be ascribed to the dominant HOMO → LUMO transition with large rotational strength, whereas the relatively weak HOMO−1 → LUMO transition in (*R*,*R*)-**2** results in a CD spectrum featuring a distinct negative component in this region.

Conclusions

Propeller-shaped molecules **1** and **2** were readily synthesized through a two-step S_NAr sequence using chiral amines. Both molecules exhibited distinct CD and CPL activities without any optical resolution, demonstrating that the intrinsic chirality of the molecular framework is sufficient to induce pronounced chiroptical responses. Although the introduction of a bifunctional linker was expected to enhance the anisotropy factor, no significant improvement was observed experimentally. DFT calculations clarified that the difference in g_{lum} values between **1** and **2** originates from the distinct orientations of their electric and magnetic transition dipole moments. Overall, this study demonstrates that the incorporation of chiral auxiliaries into a propeller-type π-conjugated scaffold effectively stabilizes its dynamic chirality. These findings offer valuable design principles for the rational development of next-generation chiroptical molecular materials.

Author contributions

M. T. and H. U. designed the project. Y. T. and R. O. performed most of the experimental works. M. T. and Y. T. prepared the overall manuscript. All authors, including T. O. and H. U., contributed by commenting on the manuscript.

Conflicts of interest

There are no conflicts to declare.

Data availability

The data supporting this manuscript can be found in its supplementary information (SI). Supplementary information: detailed synthetic procedures, NMR spectra for all new compounds, and computational details. See DOI: https://doi.org/10.1039/d5ra09136e.

Acknowledgements

The authors are grateful to Dr Kosuke Oki and Kohei Hamada for their contributions to the preliminary synthetic experiments. The authors further acknowledge Prof. Masashi Hasegawa (Kitasato Univ.) for his advice on the DFT calculations of the transition dipole moments. This work was supported by JSPS KAKENHI (JP24K01470 (M. T.), JP23H03964 (M. T.), JP20H02725 (M. T.), and JP19K05422 (H. U.)). M. T. acknowledge the Nagase Science Technology Foundation. Y. T. acknowledges JSPS Research Fellowship for Young Scientists.

Notes and references

1 D.-W. Zhang, M. Li and C.-F. Chen, *Chem. Soc. Rev.*, 2020, **49**, 1331–1343.
2 J. F. Sherson, H. Krauter, R. K. Olsson, B. Julsgaard, K. Hammerer, I. Cirac and E. S. Polzik, *Nature*, 2006, **443**, 557–560.
3 D. Zhu, W. Jiang, Z. Ma, J. Feng, X. Zhan, C. Lu, J. Liu, J. Liu, Y. Hu, D. Wang, Y. S. Zhao, J. Wang, Z. Wang and L. Jiang, *Nat. Commun.*, 2022, **13**, 3454.
4 P. Stachelek, L. MacKenzie, D. Parker and R. Pal, *Nat. Commun.*, 2022, **13**, 553.
5 Y. Shen and C.-F. Chen, *Chem. Rev.*, 2012, **112**, 1463–1535.
6 M. Rickhaus, M. Mayor and M. Juríček, *Chem. Soc. Rev.*, 2016, **45**, 1542–1556.
7 A. Bedi and O. Gidron, *Acc. Chem. Res.*, 2019, **52**, 2482–2490.
8 M. A. Majewski and M. Stępień, *Angew. Chem., Int. Ed.*, 2019, **58**, 86–116.
9 J. M. Fernández-García, P. Izquierdo-García, M. Buendía, S. Filippone and N. Martín, *Commun. Chem.*, 2022, **58**, 2634–2645.
10 S. T. Bao, S. Louie, H. Jiang, Q. Jiang, S. Sun, M. L. Steigerwald, C. Nuckolls and Z. Jin, *J. Am. Chem. Soc.*, 2024, **146**, 51–56.
11 I. Shioukhi, H. Batchu, G. Schwartz, L. Minion, Y. Deree, B. Bogoslavsky, L. J. W. Shimon, J. Wade, R. Hoffman, M. J. Fuchter, G. Markovich and O. Gidron, *Angew. Chem., Int. Ed.*, 2024, **63**, e202319318.
12 N. Saleh, B. Moore II, M. Srebro, N. Vanthuyne, L. Toupet, J. A. G. Williams, C. Roussel, K. K. Deol, G. Muller, J. Autschbach and J. Crassous, *Chem.–Eur. J.*, 2015, **21**, 1673–1681.
13 Y. Matsuo, M. Gon, K. Tanaka, S. Seki and T. Tanaka, *J. Am. Chem. Soc.*, 2024, **146**, 17428–17437.
14 F. Morita, Y. Kishida, Y. Sato, H. Sugiyama, M. Abekura, J. Nogami, N. Toriumi, Y. Nagashima, T. Kinoshita, G. Fukuhara, M. Uchiyama, H. Uekusa and K. Tanaka, *Nat. Synth.*, 2024, **3**, 774–786.
15 Y. Nakakuki, T. Hirose, H. Sotome, M. Gao, D. Shimizu, R. Li, J.-Y. Hasegawa, H. Miyasaka and K. Matsuda, *Nat. Commun.*, 2022, **13**, 1475.
16 B. Mahlmeister, M. Mahl, H. Reichelt, K. Shoyama, M. Stolte and F. Würthner, *J. Am. Chem. Soc.*, 2022, **144**, 10507–10514.
17 X. Liu, Z. Jin, F. Qiu, Y. Guo, Y. Chen, Z. Sun and L. Zhang, *Angew. Chem., Int. Ed.*, 2024, **63**, e202407547.
18 Y. Dong, Z. Zhang, Y. Hashikawa, H. Meng, F. Bai, K. Itami and Chaolumen, *Angew. Chem., Int. Ed.*, 2024, **63**, e202406927.
19 M. Gingras, G. Félix and R. Peresutti, *Chem. Soc. Rev.*, 2013, **42**, 1007–1050.
20 J. Lorkowski, D. Bouetard, P. Yorkgitis, M. Gembicky, T. Roisnel, N. Vanthuyne, D. Munz, L. Favereau,

G. Bertrand, M. Mauduit and R. Jazzar, *Angew. Chem., Int. Ed.*, 2023, **62**, e202305404.
21 P. Jiang, A. S. Mikherdov, H. Ito and M. Jin, *J. Am. Chem. Soc.*, 2024, **146**, 12463–12472.
22 S. Feuillastre, M. Pauton, L. Gao, A. Desmarchelier, A. J. Riives, D. Prim, D. Tondelier, B. Geffroy, G. Muller, G. Clavier and G. Pieters, *J. Am. Chem. Soc.*, 2016, **138**, 3990–3993.
23 M. Coehlo, L. Frédéric, L. Poulard, N. Ferdi, L. Estaque, A. Desmarchelier, G. Clavier, J.-P. Dognon, L. Favereau, M. Giorgi, J.-V. Naubron and G. Pieters, *Angew. Chem., Int. Ed.*, 2024, e202414490.
24 A. Swain, K. Radacki, H. Braunschweig and P. Ravat, *Chem. Sci.*, 2024, **15**, 11737–11747.
25 G. Ouyang, J. Rühe, Y. Zhang, M.-J. Lin, M. Liu and F. Würthner, *Angew. Chem., Int. Ed.*, 2022, **61**, e202206706.
26 N. Saleh, V. Zullo, E. Sucre-Rosales, L. Arrico, F. Zinna, G. Pescitelli, C. Besnard, E. Vauthey and J. Lacour, *Chemistry*, 2025, **31**, e202500490.
27 T. Kosaka, S. Iwai, Y. Inoue, T. Moriuchi and T. Mori, *J. Phys. Chem. A*, 2018, **122**, 7455–7463.
28 T. Kosaka, Y. Inoue and T. Mori, *J. Phys. Chem. Lett.*, 2016, **7**, 783–788.
29 M. Toyoda, Y. Imai and T. Mori, *J. Phys. Chem. Lett.*, 2017, **8**, 42–48.
30 Y. Tanioka, M. Takase, M. Hamasu, S. Hata, K. Hashimoto, S. Mori, Y. Ishibashi, Y. Nukumi, M. Higashi, H. Sato, T. Okujima and H. Uno, *Angew. Chem., Int. Ed.*, 2025, **64**, e202509190.
31 K. Shizu, J. Lee, H. Tanaka, H. Nomura, T. Yasuda, H. Kaji and C. Adachi, *Pure Appl. Chem.*, 2015, **87**, 627–638.
32 N. Blouin and M. Leclerc, *Acc. Chem. Res.*, 2008, **41**, 1110–1119.
33 M. L. S. Beaupréa, *J. Mater. Chem. A*, 2013, **1**, 11097–11105.
34 H. Uno, M. Ishiwata, K. Muramatsu, M. Takase, S. Mori and T. Okujima, *Bull. Chem. Soc. Jpn.*, 2019, **92**, 973–981.
35 Y. Sasaki, M. Takase, N. Kobayashi, S. Mori, K. Ohara, T. Okujima and H. Uno, *J. Org. Chem.*, 2021, **86**, 4290–4295.
36 T. Narita, K. Fujiwara, H. Uno, M. S. Asano, T. Nishinaga and M. Takase, *J. Porphyrins Phthalocyanines*, 2023, **27**, 1357–1363.
37 J. Chen, J. Li, L. Zhu, X. Peng, Y. Feng, Y. Lu, X. Hu, J. Liang, Q. Zhao and Z. Wang, *Org. Chem. Front.*, 2018, **5**, 3402–3405.
38 H. Uoyama, K. Goushi, K. Shizu, H. Nomura and C. Adachi, *Nature*, 2012, **492**, 234–238.
39 M. Mamada, S. Yada, M. Hayakawa, R. Uchida, H. Katagiri, T. Hatakeyama and C. Adachi, *Commun. Chem.*, 2024, **7**, 212.
40 S. T. Bao, H. Jiang, C. Schaack, S. Louie, M. L. Steigerwald, C. Nuckolls and Z. Jin, *J. Am. Chem. Soc.*, 2022, **144**, 18772–18777.